ICES Journal of Marine Science

ICES Journal of Marine Science (2018), 75(4), 1496–1508. doi:10.1093/icesjms/fsy009

Original Article

Corrections of fish school area and mean volume backscattering strength by simulation of an omnidirectional multi-beam sonar

Vasilis Trygonis[1]* and Zacharias Kapelonis[2]

[1]*University of the Aegean, Department of Marine Sciences, University Hill, Mytilene 81100, Greece*
[2]*Hellenic Centre for Marine Research, Institute of Marine Biological Resources and Inland Waters, Agios Kosmas, Athens 16777, Greece*

**Corresponding author: tel: + 30 22510 36855; e-mail: vtrygonis@marine.aegean.gr.*

Trygonis, V. and Kapelonis, Z. 2018. Corrections of fish school area and mean volume backscattering strength by simulation of an omnidirectional multi-beam sonar. – ICES Journal of Marine Science, 75: 1496–1508.

Received 13 August 2017; revised 11 January 2018; accepted 17 January 2018; advance access publication 8 March 2018.

Fish school descriptors extracted from omnidirectional multi-beam data are biased due to beam width-related effects, and echotraces are distorted in a range-dependent manner that is a function of transducer intrinsic properties, as well as fish school characteristics. This work investigates a simulation approach that models the three-dimensional insonification of fish schools by an omnidirectional fishery sonar in order to assess the bias in measuring two key morphometric and energetic descriptors, namely the horizontal cross-sectional area of schools and their mean volume backscattering strength. Simulated fish schools of different sizes and backscattering properties were insonified at various ranges from the multi-beam transducer, outputting volume backscattering strength echograms. The simulated data were used to develop empirical models that correct the examined descriptors using only information extracted from the observed echotraces. Depending on the difference between the observed mean volume backscattering strength of a school and the echogram processing threshold, mean absolute percentage errors in measured area and volume backscatter reduced from 100.7% and 79.5% to 5.2% and 6.4%, respectively. The mean volume backscattering strength of a school is a key parameter for obtaining fish density estimates, and the results highlight the need for descriptor corrections to better interpret the multi-beam data.

Keywords: beam pattern effect, bias, echotrace, fishery sonar.

Introduction

Scientific echosounders and multi-beam sonars are the primary underwater observation tools for acquiring fishery-independent data on the abundance and distribution of fish stocks (Misund, 1997; Simmonds and MacLennan, 2005). A common analysis procedure of the acoustic data is echotrace detection and classification (Reid, 2000), i.e. the processing of echograms with specialised algorithms (e.g. Weill *et al.*, 1993; Coetzee, 2000; Reid *et al.*, 2000) that extract morphometric, energetic, and positional descriptors at the fish school level.

Often complemented with auxiliary information (McClatchie *et al.*, 2000), fish school descriptors from downwards-looking echosounders find multiple uses in partitioning the acoustic data into species or target groups (Haralabous and Georgakarakos, 1996; Lawson *et al.*, 2001; Petitgas *et al.*, 2003; Fernandes, 2009), and in assessing the diel variability (Fréon *et al.*, 1996; Zwolinski *et al.*, 2007; Tsagarakis *et al.*, 2012), clustering (Petitgas *et al.*, 2001; Petitgas, 2003) and spatial structure of fish school biomass (Scalabrin and Massé, 1993; Bahri and Fréon, 2000; Castillo and Robotham, 2004). Fish school behavioural aspects such as swimming speed (Peraltilla and Bertrand, 2014), migration (Hafsteinsson and Misund, 1995; Kvamme *et al.*, 2003), and reaction to vessels or fishing and other shipboard operations (Soria *et al.*, 2003; Peña *et al.*, 2013; Stockwell *et al.*, 2013) are typically investigated with multi-beam sonars, due to the larger sampling volume of these instruments and their ability for concurrent insonification of multiple fish schools (Trygonis *et al.*, 2016) near the sea surface (Misund *et al.*, 1996). The multi-beam data per ping can also be visualized as a two-dimensional image (hereafter referred to as a "multi-beam echogram"), by arranging the acoustic samples per beam in a sonar-centred polar grid, whose across-beam resolution increases with range. School

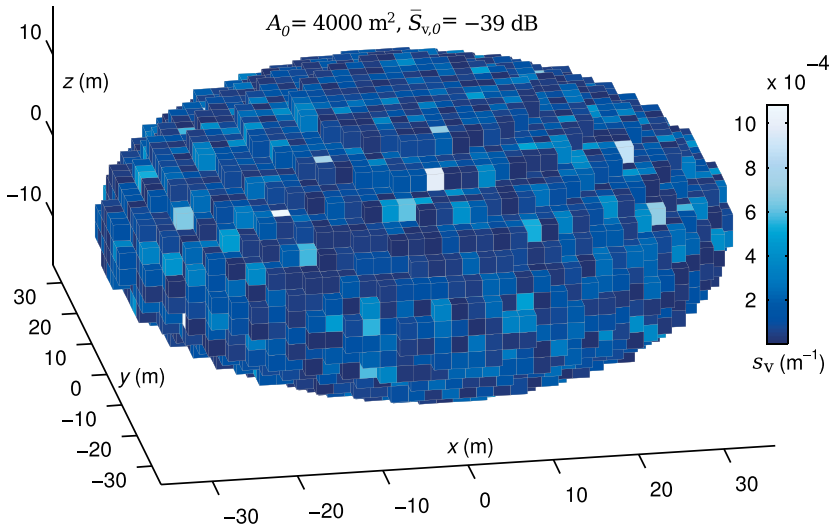

Figure 1. Example voxel school that consists of $N_k = 10\,720$ cubic voxels with identical volume ($V_{vox} = 8$ m^3) but varying volume backscattering coefficients $s_{v,k}$ that derive from an exponential distribution with $<\mu> = 10^{-39/10}$. The actual mean of the 10 720 voxel backscattering coefficients is $\bar{s}_{v,0} = 1.2676 \times 10^{-4}$ m^{-1}, corresponding to the true mean volume backscattering strength of the school $\bar{S}_{v,0} = 10\log_{10}(\bar{s}_{v,0}) = -38.970$ dB. The true maximum length along the *x*-, *y*-, *z*-axes is $(\dot{L}_{x,0}, \dot{L}_{y,0}, \dot{L}_{z,0}) = (72, 72, 32)$ m, which yields a true cross-sectional area $A_0 = 4048$ m^2 on the *x*–*y* plane at $z = 0$. To simplify notations in the main text, this school is referred to as $A_0 = 4000$ m^2, $\bar{S}_{v,0} = -39$ dB.

detection techniques are also applicable in multi-beam echograms, and range from image processing of the sonar display (Brehmer *et al.*, 2006; Uranga *et al.*, 2017) to direct manipulations of the acoustic data samples in order to isolate and measure the echotraces of interest (Gerlotto and Paramo, 2003; Trenkel *et al.*, 2009; Trygonis *et al.*, 2009).

Regardless of the acoustic platform, an inherent restriction that underlies the school detection methodologies is the impact of the insonification procedure on observed fish school properties. It has been early recognized that fish school descriptors extracted from echograms are biased by the beam pattern effect (Olsen, 1969; Johannesson and Losse, 1977), and simulation approaches have provided the means for corrections in single beam echograms (Diner, 2001, 2007). The beam width-related distortion of school echotraces and the threshold dependency of effective detections (Aglen, 1983) are also present in horizontal multi-beam measurements (Misund, 1990; Misund *et al.*, 1995), with increased complexities due to the larger ranges typically used, the angular resolution of echograms, as well as the overlap of neighbouring beams and the oblique angles under which fish are insonified (Cutter and Demer, 2007). As demonstrated by recent works (Holmin *et al.*, 2012; Vatnehol *et al.*, 2017), simulations of the multi-beam insonification procedure can greatly enhance the interpretation of echograms and provide more accurate estimates of fish school metrics.

This paper presents a fisheries acoustic simulator that models the insonification of fish schools by omnidirectional multi-beam sonar in an environment without noise or reverberation. Taking into account the range-dependent distortion of echotraces induced by the polar geometry of the echogram, the beam pattern effect, and the overlap between neighbouring beams, the study objectives are to: (a) simulate data from an omnidirectional fishery sonar that represent the insonification of fish schools of different size and density classes, observed at varying distances from the transducer; (b) assess the errors in measuring two key morphometric and energetic descriptors of fish schools, namely their horizontal cross-sectional area and mean volume backscattering strength; (c) develop empirical models which use only information extracted from the observed echotrace to correct these descriptors. The empirical models are also applied to real sonar data to examine how the predicted corrections modify the acoustic descriptors of real fish schools.

Methods

General description of the simulation

The simulator (developed in MATLAB®) implements a model of the transducer's two-way beam pattern and simulates echoes from fish schools, outputting volume backscattering strength echograms that are comparable to those produced by the real acoustic device being modelled. The virtual fish schools insonified can be customized into different sizes and backscattering properties, and can be positioned at various distances and depths relative to the transducer. Sonar operational settings such as transducer depth, observation range, and tilt angle of beams are decoupled from the insonified targets and can be modified on a ping-by-ping basis. The main assumptions of this simulation approach are that:

(i) Target echoes are incoherent, i.e. their phases are unrelated (Simmonds and MacLennan, 2005).

(ii) Acoustic extinction and multiple scattering are negligible.

(iii) The insonified school is the only source of backscatter.

(iv) Sound speed is constant throughout the propagation path.

(v) There is no noise or reverberation, nor seafloor or sea surface reflections.

The simulator was configured to implement the Simrad SP90 (Simrad, 2007), which is an omnidirectional multi-beam fishery sonar that operates at a frequency of 20–30 kHz (for research applications of the SP90, see Brehmer *et al.*, 2007, 2012; Stockwell *et al.*, 2013; Trygonis *et al.*, 2009, 2016). The sonar can be operated in two configurations, namely the "horizontal" and "vertical" transmit modes. In the horizontal mode, the SP90 provides full 360° coverage around the cylindrical transducer and all beams share the same tilt angle relative to the sea surface, forming an umbrella-shaped omnidirectional fan; echoes are received by 64 beams. The vertical mode provides a 60° wide vertical slice of the water column in a single transmission. Only the horizontal (omnidirectional) configuration was simulated in the current study, using the beam pattern corresponding to the 26 kHz continuous wave (CW) normal mode of the sonar (in this mode, the SP90 operates at a fixed signal frequency; pulse duration: 10 ms; nominal beam width: 11.25° for horizontal reception, 9° vertical).

Notations

The subscripts annotating the various quantities are as follows:

- 0: True property of a simulated fish school.
- obs: Observed descriptor of an echotrace, as extracted from the multi-beam echogram.
- CF: Correction factor of an observed descriptor.
- c: Corrected descriptor.

The "bar" and "dot" accents in descriptors (e.g. $\overline{S}_v$ and $\dot{S}_v$) denote the mean and maximum, respectively.

Fish school model

The virtual schools subjected to insonification (Figure 1) are modelled as a three-dimensional structure of adjacent cubic voxels k (volume elements) that have the same volume V_{vox} but varying volume backscattering coefficients (MacLennan *et al.*, 2002) $s_{v,k}$. For the simulations described herein, the shape of the school and the $s_{v,k}$ value per voxel k remain fixed across insonifications, and each voxel is assumed to have an omnidirectional response.

The geometric properties of a simulated school are determined by the user-defined voxel volume V_{vox}, and the nominal equatorial (α) and polar ($a' < \alpha$) radii of an oblate spheroid that represents the general school shape. To construct the school, the entire volume of the spheroid is converted into an equivalent discrete space that consists of cubic voxels of volume V_{vox} within a locally defined system of reference. This process automatically determines the total number of voxels N_k comprising the school, as well as the position of each voxel in space relative to the school-centred coordinate system. The school's true cross-sectional area A_0 (m^2) is defined as the area of the largest (equatorial) horizontal cross-section of the voxel-based structure. In terms of acoustic characteristics, each voxel is allocated a different volume backscattering coefficient $s_{v,k}$ that is pseudo-randomly drawn from the exponential distribution with mean parameter $<\mu> = 10^{<M>/10}$ (m^{-1}), where $<M>$ in dB is the nominal (expected) mean volume backscattering strength of the school, as defined by the user. The mean of these N_k exponentially distributed $s_{v,k}$ values assigned to the voxels is the true mean $\overline{s}_{v,0}$ (m^{-1}) of the school, and corresponds to the true mean volume backscattering strength $\overline{S}_{v,0} = 10\log_{10}(\overline{s}_{v,0})$ dB. Note that:

(i) the actual $\overline{S}_{v,0}$ of a school will slightly differ from the nominal value $<M>$, due to the pseudo-random sampling involved;

(ii) the school's true cross-sectional area A_0 on the equatorial (x–y) plane will slightly differ from the nominal value $\pi\alpha^2$, due to discrete nature of the school model.

To simplify notations in the remainder of this text, voxel schools will be referred to using their nominal properties $<M>$ and $\pi\alpha^2$; the actual true values will be used for all calculations.

Simulated measurement of school backscatter

Consider a school voxel k that includes n_k fish individuals and has a known true volume backscattering coefficient $s_{v,k}$. Each ith individual contained in the voxel has a different backscattering cross-section $\sigma_{bs,i,k}$ and, assuming random phases and negligible acoustic extinction, the voxel's total backscatter is the sum of all n_k fish contributions:

$$s_{v,k} = \sum_{i=1}^{n_k} \frac{\sigma_{bs,i,k}}{V_{vox}}, \tag{1}$$

where V_{vox} is the voxel's volume, which is identical for all N_k voxels that comprise the simulated school. The effective sampling volume of an acoustic sample s located at range r_s from the transducer is

$$V_{s,bm} = \frac{1}{3}\left((r_s + \Delta r/2)^3 - (r_s - \Delta r/2)^3\right)\psi_{bm}, \tag{2}$$

where the subscript bm denotes the beam index, ψ_{bm} is the equivalent beam angle in steradians, and Δr is the along-beam sample size in meters; i.e. $V_{s,bm}$ is a spherical cone shell that extends Δr in the along-beam direction and across the face of the beam to include the equivalent beam angle. This volume may contain $N_{k,s,bm}$ voxels during an insonification, and all individuals within this volume will contribute to the volume backscattering coefficient of sample s

$$s_{v,s,bm} = \frac{\sum_{k=1}^{N_{k,s,bm}} \sum_{i=1}^{n_k} \sigma_{bs,i,k}\, b_{bm}^2(\theta_{i,k,bm}, \phi_{i,k,bm})}{V_{s,bm}}, \tag{3}$$

where $b_{bm}^2(\theta_{i,k,bm}, \phi_{i,k,bm})$ is the two-way beam pattern regarding the ith individual within voxel k. The external sum in Equation (3) adds across the $N_{k,s,bm}$ voxels that can contribute backscatter to sample s, while the internal one sums the backscattering cross-sections within these voxels, weighted by the beam pattern. Here, the beam angles $\theta_{i,k,bm}$ and $\phi_{i,k,bm}$ are referenced to the acoustic axis and operate on the orthogonal directions that correspond to the vertical (elevation) and horizontal (azimuth) aspect of the beam, respectively. Assuming that the beam angle differences for all individuals within a specific voxel are negligible, $\theta_{i,k,bm}$ and $\phi_{i,k,bm}$ can be replaced with $\theta_{k,bm}$ and $\phi_{k,bm}$, respectively, i.e. the elevation and azimuth angle of the voxel's geometric centre relative to the acoustic axis of beam bm. Combining Equations (1), (2), and (3) results in the following expression that describes the volume backscattering coefficient measured by the simulator:

$$s_{v,s,bm} = \frac{V_{vox} \sum_{k=1}^{N_{k,s,bm}} s_{v,k}\, b_{bm}^2(\theta_{k,bm}, \phi_{k,bm})}{\frac{1}{3}\left((r_s + \Delta r/2)^3 - (r_s - \Delta r/2)^3\right)\psi_{bm}}; \tag{4}$$

i.e. for each insonification, the volume backscattering strength $S_{v,s,bm} = 10\log_{10}(s_{v,s,bm})$ of each sample s in the simulated

echogram is calculated as the weighted sum of the (known) volume backscattering coefficients $s_{v,k}$ of the $N_{k,s,bm}$ voxels that effectively contribute backscatter to $V_{s,bm}$. In order to acquire $N_{k,s,bm}$, the simulator selects the voxels whose radial position r_k is $(r_s - \Delta r/2 < r_k \leq r_s + \Delta r/2)$, and, to reduce unnecessary computations on voxels whose backscatter is practically nulled by the beam pattern, it filters out any voxels that have angular position $\theta_{k,bm}$ and/or $\phi_{k,bm}$ greater than five times the full beam width bw_θ and bw_φ, respectively. If a voxel k contributes to more than one range-ring of the echogram (i.e. it spans across multiple samples in the along-beam direction), Equation (4) is modified for that k by replacing V_{vox} with $v_{k,s}$, where $v_{k,s}$ is the approximate portion of the voxel's volume that falls within sample s $(0 < v_{k,s} < V_{vox})$; to perform the latter calculations, it is temporarily assumed that the voxel's face is normal to the acoustic axis and the samples have a planar (instead of a spherical) face in the along-beam direction.

For each simulated insonification, the position of school voxels relative to the sonar beams is assumed to be constant between transmission and reception.

Transducer model

The beam pattern of the SP90 transducer was manually digitized from the sonar manufacturer diagrams (26 kHz, normal mode, see Brehmer *et al.*, 2007 and sources therein) with a 0.5° step over the [–25°, +25°] domain centred to the acoustic axis. Digitization of the beam pattern was performed separately for the horizontal (b_h) and vertical (b_v) aspect, and piecewise cubic hermite interpolating polynomials (PCHIP) (Fritsch and Carlson, 1980) were used to model b_h and b_v as a function of the beam angles ϕ_k and θ_k, respectively. The shape of only one beam was mapped as described, and its directivity was applied to all beams of the simulated omnidirectional fan.

Note that, when operating in the horizontal mode simulated here, the sonar is directive in the horizontal aspect during reception, but the overall transmitted wave is omnidirectional when viewed as a projection on a horizontal plane. Therefore, for each beam, the two-way beam pattern used by the simulator in the horizontal (azimuth) aspect is

$$b_h(\phi_k) = b_h^{Tx}(\phi_k)\, b_h^{Rx}(\phi_k), \tag{5}$$

where $b_h^{Tx}(\phi_k) = 1\ \forall \phi_k$, and the two-way directivity in the vertical (elevation) aspect is

$$b_v(\theta_k) = b_v^{Tx}(\theta_k)\, b_v^{Rx}(\theta_k), \tag{6}$$

where $b_v^{Tx}(\theta_k) = b_v^{Rx}(\theta_k)$. Superscripts Tx and Rx in Equations (5) and (6) denote transmission and reception, respectively, while the parameters $b_h^{Rx}(\phi_k)$ and $b_v^{Tx}(\theta_k)$ are the output of the PCHIP model. According to these definitions, the two-way beam pattern used in Equation (4) is

$$b_{bm}^2(\theta_k, \phi_k) = b_v(\theta_k)\, b_h(\phi_k) \tag{7}$$

and is assumed identical for all beams bm. The equivalent beam angle ψ_{bm} was estimated from the integral of the entire beam pattern over the hemisphere in front of the beam (Simmonds and MacLennan, 2005).

Simulated scenarios

The stationary transducer was configured to simulate the SP90 sonar and was positioned at $(x, y, z) = (0, 0, -4\,m)$ in the global Cartesian coordinate system. Sonar observation range was set to 900 m, and beam tilt angle was –5° below the horizon. The sonar was subsequently rotated about the vertical so that, when projected on the x–y plane, the acoustic axis of a beam was aligned with the $+x$-axis (starboard side). The transducer placement and insonification settings remained fixed throughout the simulations.

Ten school size classes were created, characterized by their true maximum horizontal cross-sectional area (A_0) that ranged from 1000 to 10 000 m^2. Ten different true mean volume backscattering strength ($\overline{S}_{v,0}$) classes were allocated per school size class, producing 100 simulated schools in total (Table 1); voxel volume V_{vox} was 8 m^3 ($2 \times 2 \times 2$ m) for all schools. During the simulations, the geometric centre of a school was incrementally positioned at $(x, y, z) = (X_{G,0,n}, 0, Z_{G,0})$ in the global Cartesian coordinate system, where the subscript n denotes the nth insonification and $Z_{G,0}$ is the school depth. Depending on school size class, $Z_{G,0}$ varied between –25 and –35 m to accommodate the school's width in the vertical dimension. Considering this positioning setup, the $X_{G,0,n}$ coordinate practically governs the school's distance from the transducer, and was set to $X_{G,0,n} = 100 + 20(n - 1)$ m, where $n \in [1, 2, \ldots, 36]$. Only one school was present in the simulated world per insonification, and $Z_{G,0}$ remained constant as a specific school was translated (with no rotation) away from the transducer.

Extraction of simulated fish school descriptors

A range of cut-off thresholds T (–53 to –47 dB, in steps of 1 dB) were applied on each simulated echogram, and a series of morphometric, energetic, and positional echotrace descriptors were extracted per threshold level, using the multi-beam school detection algorithm described in Trygonis *et al.* (2009). Echotraces consisting of ≤ 10 echogram samples were excluded from all further analyses. Based on these simulation results, where both the true properties of the schools and the observed echotrace descriptors were known, (observed) correction factors were calculated per threshold level T to assess the systematic bias on school horizontal area and mean volume backscattering strength. Specifically, the area correction factor A_{CF} was defined as the dimensionless number that the observed echotrace area must be multiplied with, in order to match the true value: $A_0 = A_{obs} \times A_{CF}$. For the logarithmic mean volume backscattering strength of the school, the correction factor $\overline{S}_{v,CF}$ was defined as the difference (in dB) between the observed and the true value: $\overline{S}_{v,CF} = \overline{S}_{v,obs} - \overline{S}_{v,0}$. Accordingly, $A_{CF} < 1$ denotes overestimation of the true school area, while $\overline{S}_{v,CF} < 0$ corresponds to underestimation of the true school density.

Development of correction models

After calculating the observed correction factors, multiple linear regression models were developed in order to investigate the ability to predict the true mean S_v and true area of a school (i.e. predict the correction factors) using only descriptors extracted from the school's echotrace. The underlying hypothesis is that, once all sources of bias that are intrinsic to the system are in effect, including the systematic distortions over the nominal echogram geometry, the resulting echotrace retains enough information to

Table 1. Summary of simulated scenarios, listing the stationary transducer settings, the true properties of the simulated schools, and their position on the global Cartesian coordinate system.

Transducer properties					
Range	**Position**		**Tilt**		
900 m	$(x, y, z) = (0, 0, -4)$ m		-5°		
School properties					
A_0 (m^2)	$\overline{S}_{v,0}$ (dB)	$\dot{L}_{x,0}$ (m)	$\dot{L}_{y,0}$ (m)	$\dot{L}_{z,0}$ (m)	$Z_{G,0}$ (m)
1000	[−42, . . ., −33][a]	36	36	18	−25
2000	[−42, . . ., −33][a]	48	48	24	−25
3000	[−42, . . ., −33][a]	60	60	26	−28
4000	[−42, . . ., −33][a]	72	72	32	−28
5000	[−42, . . ., −33][a]	80	80	36	−30
6000	[−42, . . ., −33][a]	88	88	38	−30
7000	[−42, . . ., −33][a]	96	96	40	−32
8000	[−42, . . ., −33][a]	100	100	42	−32
9000	[−42, . . ., −33][a]	108	108	44	−35
10 000	[−42, . . ., −33][a]	112	112	46	−35
School position					
$(x, y, z) = (X_{G,0}, 0, Z_{G,0})$, where $X_{G,0} = [100, \ldots, 800]$ in steps of 20 m					

Voxel backscattering coefficients are exponentially distributed and average at $\overline{S}_{v,0}$ when expressed in dB. $\dot{L}_{x,0}$, $\dot{L}_{y,0}$, $\dot{L}_{z,0}$ represent the maximum school width along the *x*-, *y*-, *z*-axis, respectively; $Z_{G,0}$ is the depth of the geometric centre of the school; A_0 is the school area at the largest horizontal cross-section, i.e. on the *x*–*y* plane at $z = Z_{G,0}$.
[a]In steps of 1 dB.

statistically infer the true properties of the school with a sufficient level of confidence.

To this end, separate models were built for $\overline{S}_{v,CF}$ and A_{CF}, in which the correction factor was the dependent variable and predictors were the school range ($R_{G,obs}$, m), the number of school echotrace samples (ns_{obs}), the area (A_{obs}, m^2), the maximum along-beam ($\dot{L}w_{obs}$, m) and across-beam width (Cw_{obs}, m), the ratio $\dot{L}w_{obs}/R_{G,obs}$, the mean ($\overline{S}_{v,obs}$, dB), max ($\dot{S}_{v,obs}$,dB) and sum ($\Sigma S_{v,obs}$, dB) volume backscattering strength, and the log standard deviation of the volume backscattering coefficients of school echotrace samples [$\log_{10}(\sigma s_{v,obs})$, m^{-1}]; see Trygonis *et al.* (2009) for details on the calculations of school descriptors. Note that $\overline{S}_{v,obs}$ and $\Sigma S_{v,obs}$ are computed using the linear volume backscattering coefficients of an observed echotrace, and then transformed to dB (MacLennan *et al.*, 2002). Statistically non-significant ($p > 0.05$) predictors were removed from each regression model, and the latter were rebuilt.

The $\overline{S}_{v,CF}$ and A_{CF} prediction models were developed on training data and validated against unknown (testing) ones. Note that, in order to assess the limitations of this descriptor correction approach in echotraces of low $\overline{S}_{v,obs}$, several candidate multiple linear regression models were initially built using training data with varying $\Delta\overline{S}_T = \overline{S}_{v,obs} - T$, i.e. with varying difference (in dB) between the observed mean volume backscattering strength of a school and the cut-off threshold. Specifically, all available simulated data (i.e. 100 voxel schools of varying A_0 and $\overline{S}_{v,0}$, each insonified at different distances $X_{G,0}$ and incrementally processed with seven thresholds T) were pooled, and then filtered by increasing levels of $\Delta\overline{S}_T$ ($\geq$ 0, 1, 2, 3, 4, 5, and 6 dB). Within each $\Delta\overline{S}_T$ pool, stratified random sampling was performed with a 50–50% partitioning scheme: for each unique combination of [$\overline{S}_{v,0}$, A_0, T], the insonification distance $X_{G,0}$ was split into [140–240, 260–360, . . ., 620–720, 740–800 m] bins, and 50% of echotraces falling within each $X_{G,0}$ bin were randomly selected and moved to the training data set, while the other 50% were moved to the testing one. This produced seven preliminary training/testing data sets (one per $\Delta\overline{S}_T$ level), within which the relative proportion of $\overline{S}_{v,0}$, A_0, $X_{G,0}$, and T instances was maintained, but without any common cases between training and testing data. One $\overline{S}_{v,CF}$ and one A_{CF} candidate prediction model was then built per $\Delta\overline{S}_T$ training data set, and was applied to the respective testing data. The candidate models built from the lowest $\Delta\overline{S}_T$, which produced consistent prediction performance with all higher $\Delta\overline{S}_T$ models were selected as the final correction models presented herein.

Note that the two smallest $X_{G,0} = [100, 120\,\text{m}]$ classes were omitted from all models (and subsequent corrections). This was based on a preliminary analysis, which showed that, due to the fact that the largest portion of the school—or its entirety—was outside the tilted acoustic beams at such short distances from the transducer, the inclusion of these few, insufficiently sampled by the sonar, echotraces reduced the performance of all candidate $\overline{S}_{v,CF}$ and A_{CF} models.

Results

The insonification of the 100 simulated schools across 36 different positions relative to the stationary transducer (Table 1) produced 3600 cases per threshold level T, yielding a total of 25 200 simulated pings that helped investigate the variability in the observed descriptors. To facilitate the presentation, detailed results are initially shown for the simulation scenarios processed with $T = -51$ dB; the analysis of the total simulation output is presented further below in this section.

Simulation scenarios processed with threshold −51 dB

Figure 2a and e shows the simulated echograms of two schools that have identical true geometric characteristics, but different true mean volume backscattering strength, insonified at various distances from the stationary transducer. Selected geometric and energetic descriptors of the observed echotraces and their relation to the respective true values are plotted in Figure 2c–d and g–h.

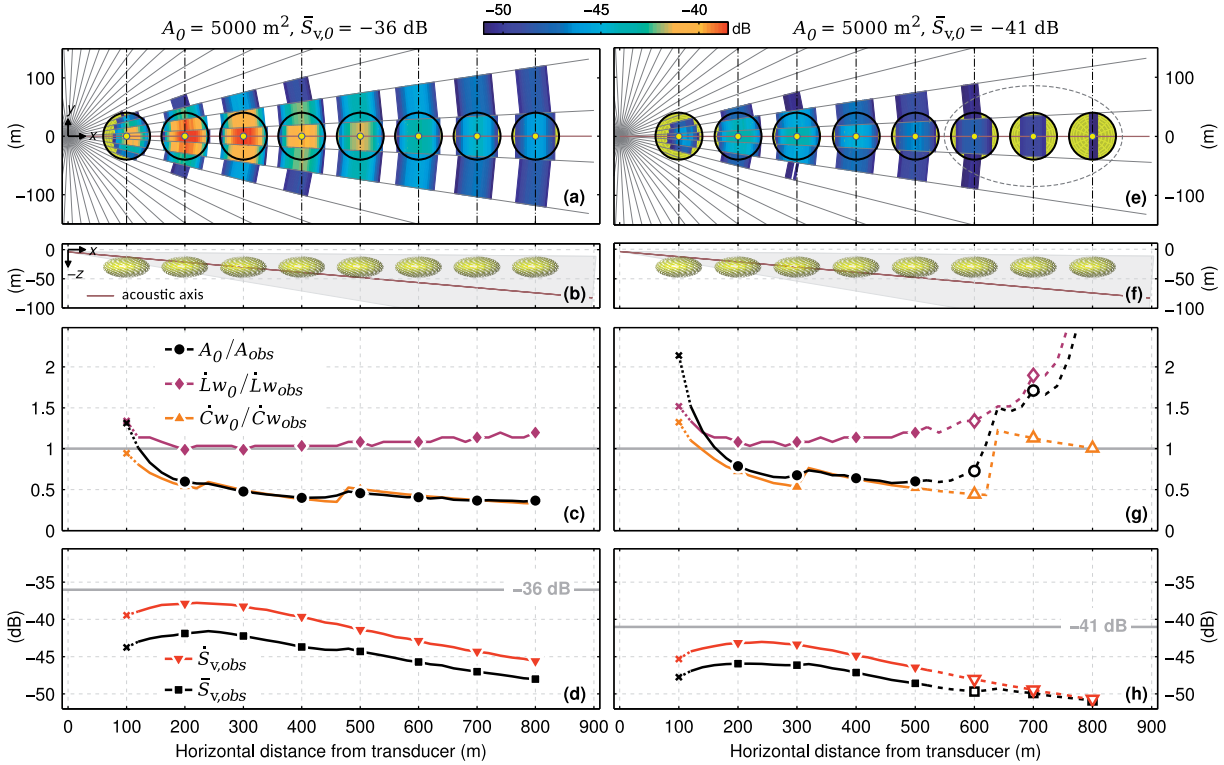

Figure 2. (a) Simulated echotraces of a school with true area $A_0 = 5000$ m^2 and true mean volume backscattering strength $\bar{S}_{v,0} = -36$ dB insonified at various distances from the stationary transducer, and processed with a threshold $T = -51$ dB; the intermediate insonifications at $X_{G,0} = [120, 140, 160, 180, 220, \ldots, 780$ m] are not shown. At each insonification position, the projection of the school's geometric centre on the x–y plane is denoted with a closed marker, and a circle marks the school's outer boundary. (b) x–z view of the simulated scenario. The sonar beams are tilted at −5°, the transducer depth is −4 m, and the depth of the school's geometric centre is constant at $Z_{G,0} = -30$ m; the grey patch represents the acoustic beam that is aligned with the +x-axis. (c) Observed geometric echotrace descriptors vs. the respective true properties. (d) Observed maximum ($\dot{S}_{v,obs}$) and mean ($\bar{S}_{v,obs}$) volume backscattering strength; the horizontal line at −36 dB denotes the true mean. (e–h) As in panels a–d, but for a school with the same true area and lower $\bar{S}_{v,0}$ (= −41 dB). The dashed ellipse in panel e and the dashed lines with open markers in panels g and h denote echotraces with $\Delta\bar{S}_T < 2$ dB (i.e. $\bar{S}_{v,obs} < -49$ dB), which could not be corrected with the final $\bar{S}_{v,CF}$ and A_{CF} and prediction models. The "x" markers and dotted lines in panels c, d, g, and h show the observations at $X_{G,0} = [100, 120$ m], which were omitted from all analyses.

The simulation examples of Figure 2 demonstrate the angular and range-dependent distortion of echotraces, i.e. the smearing of the echotrace of a school over the span of all beams that fully or partially contain it (see also Figure 2 in Vatnehol *et al.*, 2017 for a schematic illustration of this distortion). The number of beams that effectively sample the school at a given range also varies, and depends on beam directivity, the processing threshold, the density of the school, and its position within the acoustic sampling volume. This smearing effect has small impact on the along-beam width of the school (Lw_{obs}), but it typically leads to the overestimation of the across-beam width (Cw_{obs}, about 50–100% at 200 m from the transducer), which is the primary contributor to the respective overestimation in the observed school area. Conversely, the average density of the school is systematically underestimated (Figure 2d and h). Low S_v samples at the periphery of the school lower the overall computed mean, while, as in single-beam echosounding (Diner, 2001), the bias further increases with range, as the school fills up a smaller proportion of the—progressively larger—acoustic sampling volume; this also applies to the central beam(s) that insonify the school, depending on the beam tilt angle and the school's true depth and size. Moreover, schools at very short distances to the transducer are severely under-sampled.

Summarizing the scenarios processed with threshold $T = -51$ dB, Figure 3 shows the observed mean volume backscattering strength ($\bar{S}_{v,obs}$) and area (A_{obs}) of simulated echotraces; the same values expressed as relative percentage errors δ are plotted in Supplementary Figure S1. The results show that the $\bar{S}_{v,obs}$ extracted from the echogram always underestimates the true value $\bar{S}_{v,0}$, and does so by a magnitude of 4–16 dB (off-axis insonifications included), depending on the range, the true size, and the true density of the school. Overall, smaller schools fall below the detection threshold at closer ranges to the transducer, and for the same $\bar{S}_{v,0}$ class, they are susceptible to a stronger underestimation of their true density and larger relative errors in their observed area (A_{obs}). For the tilted omnidirectional scenarios considered herein, the variability of A_{obs} is also greater in smaller schools, as the same target that maintains a constant depth is observed at different distances from the transducer (Supplementary Figure S1e–h). It can be suggested that for these insonification conditions, a favourable school observation range is about 150–300 m.

For each combination of ($\bar{S}_{v,0}$, A_0, distance from transducer) plotted in Figure 3, the deviation between the observed and the known true value was used to compute an observed correction factor for the mean volume backscattering strength and area ($\bar{S}_{v,CF}$ and A_{CF}, respectively). Note that echotraces with

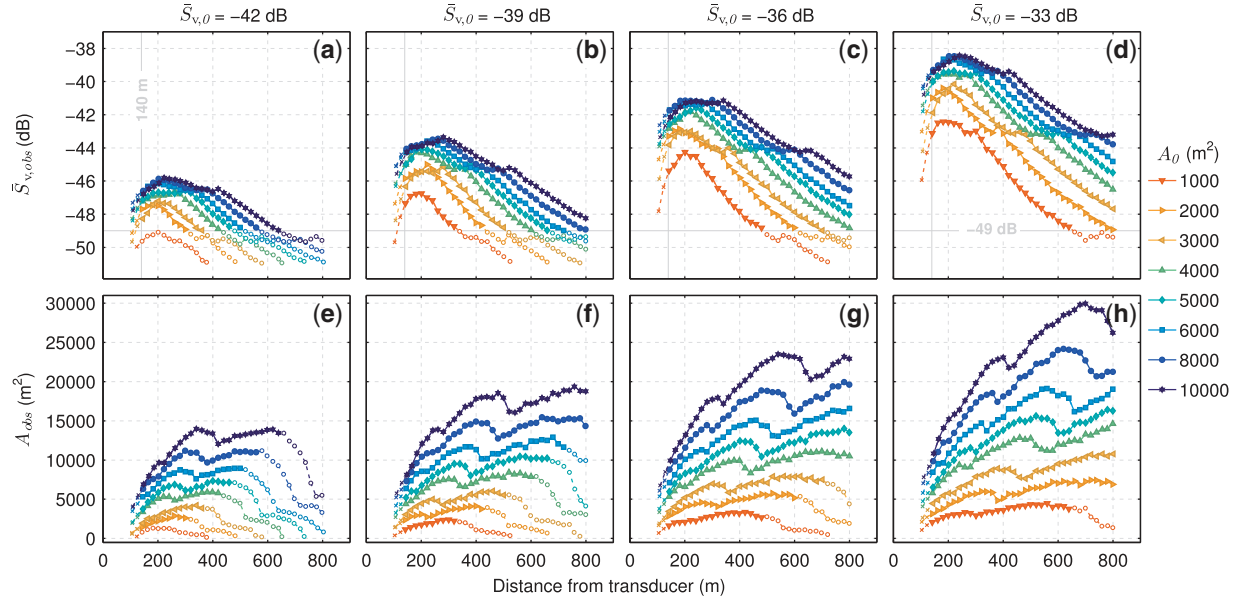

Figure 3. (a–d) Observed mean volume backscattering strength $\bar{S}_{v,obs}$ and (e–h) area A_{obs} of simulated schools vs. their distance from the transducer (training and testing data pooled), tabulated by true $\bar{S}_{v,0}$ and A_0. Threshold T is −51 dB. The $\bar{S}_{v,0} = [-41, -40, -38, -37, -35, -34$ dB] and $A_0 = [7000, 9000$ m^2] classes are not plotted to reduce clutter. Dashed lines with open markers denote echotraces with $\Delta\bar{S}_T < 2$ dB (i.e. $\bar{S}_{v,obs} < -49$ dB, marked by the horizontal line in panels a–d), which could not be corrected with the final $\bar{S}_{v,CF}$ and A_{CF} and prediction models. The "x" markers and dashed lines show the observations at $X_{G,0} = [100, 120$ m], which were omitted from all analyses (i.e. $X_{G,0} < 140$ m, marked by the vertical line in panels a–d).

$\Delta\bar{S}_T < 2$ dB (i.e. with $\bar{S}_{v,obs} < -49$ dB, shown with open markers in Figure 3) were maintained in the data set, but were eventually excluded from the final, model-based corrections. This was based on the output of all simulations analysed (see the respective section below), which showed that, for all examined processing thresholds T, echotraces with $\bar{S}_{v,obs}$ comparable to T and/or Cw_{obs} comparable to the beam width (examples shown in Figure 2e) could not be sufficiently corrected with the final $\bar{S}_{v,CF}$ and A_{CF} and prediction models. Similarly, under-sampled schools that were detected at very short distances from the transducer ($X_{G,0} = [100, 120$ m], corresponding to $R_{G,obs}$ of about < 130 m) were omitted from all analyses.

The observed correction factors $\bar{S}_{v,CF}$ and A_{CF} are plotted in Figure 4, and represent the exact corrections that must be applied to the respective echotrace descriptors when the true properties of the school are known. In practical applications, however, the true properties are not known, and the only information available about the insonified school is its acoustic image displayed in the multi-beam echogram.

Analysis of the entire simulation

Following the same procedures described above for $T = -51$ dB, all simulation scenarios listed in Table 1 were processed with a range of additional cut-off thresholds T (–53, –52, –50, –49, –48, and –47 dB), and the school detector was run for each threshold level; the echotraces were then tabulated according to their $\Delta\bar{S}_T$ (≥ 0, 1, 2, 3, 4, 5, and 6 dB) and split into stratified training/testing data sets. Separate $\bar{S}_{v,CF}$ and A_{CF} candidate prediction models were built per $\Delta\bar{S}_T$ training set, in order to investigate the range of $\Delta\bar{S}_T$ values at which the correction method should not be used.

The results are summarized in Table 2, shown as adjusted R^2 values of the candidate models and as mean absolute percentage errors $|\delta|$ (mean ± SD) of the corresponding corrections performed on the respective (i.e. same $\Delta\bar{S}_T$) testing data; the errors $|\delta|$ for mean volume backscatter were computed using the linear coefficients ($|\delta\bar{s}_{v,c}| = |\bar{s}_{v,c} - \bar{s}_{v,0}|/\bar{s}_{v,0} \times 100$). The results show that the two lowest $\Delta\bar{S}_T$ data sets (≥ 0 and ≥ 1 dB) had poor correction performance; their mean percentage errors were almost double for $|\delta\bar{s}_{v,c}|$ than all other $\Delta\bar{S}_T$ cases (e.g. 9.4 ± 7.9% for $\Delta\bar{S}_T \geq 0$ dB and 6.4 ± 6.0% for $\Delta\bar{S}_T \geq 2$ dB), and were almost triple for $|\delta A_c|$, reaching up to 13.6 ± 12.0% for $\Delta\bar{S}_T \geq 0$ dB.

Overall, Table 2 shows that filtering-out echotraces with low $\bar{S}_{v,obs}$ (i.e. keeping only the high $\Delta\bar{S}_T$ cases) significantly improved the correction performance. For example, the correction models built from the $\Delta\bar{S}_T \geq 6$ dB testing echotraces achieved a mean $|\delta\bar{s}_{v,c}|$ and $|\delta A_c|$ error of 4.6 ± 4.4% and 3.3 ± 2.7%, respectively, when applied to the corresponding testing data. The higher the $\Delta\bar{S}_T$ filter, however, the more echotraces are removed out of the usable data set. While the selection of a $\Delta\bar{S}_T$ criterion other than ≥ 0 and ≥ 1 is largely an *ad hoc* decision, a compromise appears to be $\Delta\bar{S}_T \geq 2$ dB; here, a large pool of simulated data is maintained to build the correction models (thus avoiding over-fitting the higher $\Delta\bar{S}_T$ subsets), the variability of $|\delta\bar{s}_{v,c}|$ and $|\delta A_c|$ errors drops significantly when compared to the two lower $\Delta\bar{S}_T$ sets, and is the lowest $\Delta\bar{S}_T$ at which the mean errors $|\delta|$ and adjusted R^2 values appear to stabilize.

Based on these criteria, the $\bar{S}_{v,CF}$ and A_{CF} prediction models built from, and applicable to, echotraces with $\Delta\bar{S}_T \geq 2$ dB were selected as the final ones, and are listed in Table 3. Both models use only descriptors extracted from the observed echotraces as predictive variables, and they explain more than 96% of the variance in their training data set ($N = 8618$ simulated echotraces) with a standard error of 0.379 dB for $\bar{S}_{v,CF}$ and 0.040 for A_{CF}.

When the models of Table 3 were applied to the $\Delta\bar{S}_T \geq 2$ dB testing data ($N = 8601$), relative percentage errors δ in the observed

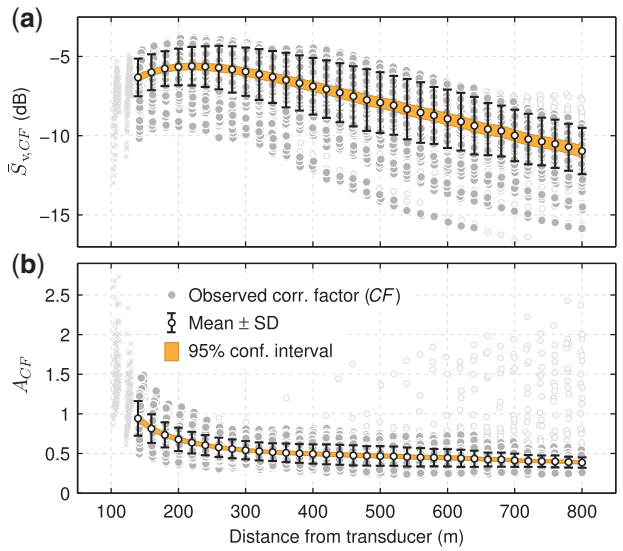

Figure 4. Observed correction factors for the (a) mean volume backscattering strength and (b) area of simulated echotraces (training and testing data pooled) vs. the school distance from the transducer. Threshold T is −51 dB. Each observed correction factor corresponds to a data point plotted in Figure 3, with the addition of all $\overline{S}_{v,0}$ and A_0 classes that were not shown therein, and is marked respectively: closed markers denote echotraces with $\Delta\overline{S}_T \geq 2$ dB ($N = 2708$), open markers correspond to echotraces with $\Delta\overline{S}_T < 2$ dB ($N = 318$), and "x" markers ($N = 196$) show the observations at $X_{G,0} = [100, 120\text{ m}]$, which were omitted from all analyses. The overlaid mean and its confidence interval per distance category refer to the $\Delta\overline{S}_T \geq 2$ dB data points only, and were estimated after bootstrapping ($\alpha = 0.05$, 10 000 resamples with replacement); error bars show the standard deviation.

Table 2. Performance of 14 candidate multiple linear regression models for predicting the mean volume backscattering strength and area correction factors ($\overline{S}_{v,CF}$ and A_{CF}, respectively).

$\Delta\overline{S}_T$ (dB)	$\overline{S}_{v,CF}$ Adj. R^2	$\lvert\delta\overline{s}_{v,c}\rvert$ %	A_{CF} Adj. R^2	$\lvert\delta A_c\rvert$ %	N
≥0	0.951	9.4 ± 7.9	0.905	13.6 ± 12.0	10031
≥1	0.952	9.2 ± 7.9	0.882	13.4 ± 11.6	9910
≥2[a]	0.974	6.4 ± 6.0	0.966	5.2 ± 4.8	8601
≥3	0.975	5.8 ± 5.3	0.971	4.4 ± 3.9	7555
≥4	0.975	5.4 ± 5.0	0.973	4.0 ± 3.3	6484
≥5	0.975	5.0 ± 4.7	0.974	3.6 ± 3.1	5321
≥6	0.977	4.6 ± 4.4	0.976	3.3 ± 2.7	4137

Each candidate model is built from training data that encompass simulated echotraces that fulfil the specific $\Delta\overline{S}_T$ criterion. The mean absolute percentage errors $\lvert\delta\rvert$ (mean ± SD) refer to the performance of models on the corresponding testing data. Volume backscatter errors $\lvert\delta\rvert$ were computed using the linear ($\overline{s}_v$) coefficients; N shows the echotrace count per testing data set, $p < 0.001$ for all models (see also Supplementary Table S1 for the performance of preliminary candidate models that include the two smallest $X_{G,0} = [100, 120\text{ m}]$ classes, which were omitted from all analyses presented herein).
[a]Models selected as "final" and listed in Table 3.

mean volume backscatter and area of simulated echotraces decreased significantly, and were normally distributed around 0% (Figure 5). In terms of mean absolute percentage errors, $\lvert\delta\overline{s}_{v,obs}\rvert$ averaged at 79.5 ± 9.6% (percentiles $P_{5\%}$–$P_{95\%}$: 63.1–93.4%) and dropped to $\lvert\delta\overline{s}_{v,c}\rvert = 6.4 \pm 6.0\%$ (Table 2) after correction ($P_{5\%}$–$P_{95\%}$: 0.5–19.1%); the respective $\lvert\delta\overline{s}_{v,c}\rvert$ errors in the $\Delta\overline{S}_T \geq 2$ dB training data ($N = 8618$) were 6.3 ± 5.9%. With respect to area, errors in the testing data were $\lvert\delta A_{obs}\rvert = 100.7 \pm 65.2\%$ ($P_{5\%}$–$P_{95\%}$: 10.9–220.0%) and reduced to $\lvert\delta A_c\rvert = 5.2 \pm 4.8\%$ ($P_{5\%}$–$P_{95\%}$: 0.4–13.7%) after corrections; in the $\Delta\overline{S}_T \geq 2$ dB training data, $\lvert\delta A_c\rvert$ was 5.1 ± 4.7%.

To further investigate the variability of corrections in the testing data set across different true school properties and processing thresholds, Table 4 lists the tabulation of $\lvert\delta\overline{s}_{v,c}\rvert$ and $\lvert\delta A_c\rvert$ by selected thresholds T and $\overline{S}_{v,0}$ and A_0 classes. The results show that the mean difference between the corrected and true $\overline{S}_v$ was 0.1–0.5 dB for most cases, while area mean absolute percentage errors typically averaged around 4–8% for most true size and density classes examined. Errors $\lvert\delta\rvert$ of the corrected descriptors were generally similar across increasing school sizes, with the exception of the smallest schools ($A_0 = 1000\text{ m}^2$) for which the corrections did not perform so adequately; $\lvert\delta\overline{s}_{v,c}\rvert$ and $\lvert\delta A_c\rvert$ of these echotraces was 11.8 ± 8.0% and 10.6 ± 9.5%, respectively (Table 4, "All $\overline{S}_{v,0}$" row). It is also worth noting that increasing the processing threshold for large schools of low true density degrades the corrections, especially those of volume backscatter, but improves them, especially the corrections of area, for denser schools of the same size class (see the $A_0 = 10\,000\text{ m}^2$ column in Table 4 for the $\overline{S}_{v,0} = -42$ and −33 dB cases, processed with different thresholds).

Application to real sonar data

The descriptor correction approach investigated in this study was applied to real SP90 data recorded around a drifting fish aggregating device (FAD) in the western Indian Ocean (see Trygonis *et al.*, 2016 and sources therein for details on data collection methods). The data originate from a recording session carried out with similar sonar settings as to those used in the simulated scenarios (horizontal omnidirectional mode at 26 kHz; observation range: 900 m; beam tilt: −3°; automatic gain control filter: off), and regard the consecutive observations of a single school of large pelagic (tuna) fish with compact echotraces that also fell within the simulated envelop (2–5-min gaps exist in the records due to vessel manoeuvres around the FAD). The scientific output of the uncalibrated sonar was analysed with custom software (Trygonis *et al.*, 2009) that implements the same school detector used to process the simulated echograms. The cut-off threshold T during school detection was set to −51 dB, and the correction models listed in Table 3 were applied to real echotraces with $\Delta\overline{S}_T \geq 2$ dB.

The results are summarized in Figure 6, and show that, on an average, the corrections increased the estimated mean volume backscattering strength of real schools by 11.3 dB (mean $\overline{S}_{v,obs} = -45.5$ dB, mean $\overline{S}_{v,c} = -34.2$ dB; Figure 6e) and reduced their estimated mean area by 68.7% (mean $A_{obs} = 3766.0\text{ m}^2$, mean $A_c = 1180.4\text{ m}^2$; Figure 6f). When plotted against their distance from the transducer (Figure 7), the observed and corrected real data show similar patterns as those produced by the simulator (Supplementary Figure S2). Specifically, the sonar systematically under-samples the low density schools with increasing range (i.e. only the denser instances are detected at large distances from the transducer), and, simultaneously with this sampling bias, the observed $\overline{S}_v$ of a detected school is an underestimate of its respective true value. Moreover, assuming that the true school area is independent from range, the results suggest that the corrections

Table 3. Final multiple linear regression models for predicting the mean volume backscattering strength and area correction factors ($\overline{S}_{v,CF}$ and A_{CF}, respectively), built from the $\Delta\overline{S}_T \geq 2$ dB training data set ($N = 8618$ simulated echotraces).

Dependent	Adjusted R^2		S.E. of the estimate		Dependent	Adjusted R^2		S.E. of the estimate	
$\overline{S}_{v,CF}$	0.974		0.379		A_{CF}	0.966		0.040	
Predictors	***B***	**S.E. *B***	***b***	**S.E. *b***	**Predictors**	***B***	**S.E. *B***	***b***	**S.E. *b***
(constant)			−23.351291	0.217	(constant)			−1.465251	0.028
$\Sigma S_{v,obs}$	2.060	0.026	1.113656	0.014	$\log_{10}(\sigma s_{v,obs})$	−3.711	0.033	−2.218302	0.020
$\log_{10}(\sigma s_{v,obs})$	−1.579	0.016	−10.183501	0.101	$\dot{S}_{v,obs}$	1.797	0.051	0.125210	0.004
$R_{G,obs}$	−1.327	0.006	−0.017038	0.000	$\Sigma S_{v,obs}$	1.255	0.030	0.062886	0.002
$\dot{L}w_{obs}/R_{G,obs}$	−0.627	0.008	−11.629761	0.157	ns_{obs}	−1.015	0.010	−0.005403	0.000
$\dot{L}w_{obs}$	0.521	0.011	0.057721	0.001	$\dot{L}w_{obs}/R_{G,obs}$	0.991	0.010	1.702406	0.017
ns_{obs}	−0.496	0.009	−0.028484	0.000	$R_{G,obs}$	−0.845	0.007	−0.001006	0.000
$\overline{S}_{v,obs}$	−0.092	0.013	−0.081974	0.011	A_{obs}	0.650	0.011	0.000025	0.000
A_{obs}	0.074	0.009	0.000030	0.000	$\overline{S}_{v,obs}$	0.416	0.025	0.034432	0.002
Cw_{obs}	−0.051	0.006	−0.002091	0.000	Cw_{obs}	0.238	0.007	0.000909	0.000
					$\dot{L}w_{obs}$	−0.199	0.013	−0.002044	0.000

Excluding *b*, values are rounded to the third decimal.
B and *b* are the standardized and raw regression coefficients, respectively; $p < 0.001$ for both models.

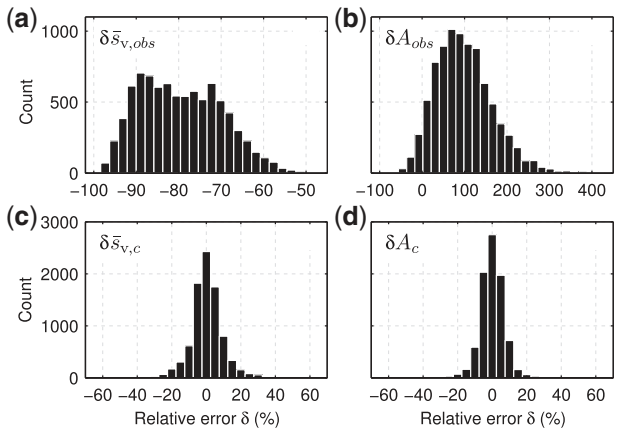

Figure 5. Distribution of relative percentage errors δ in the mean volume backscatter ($\bar{s}_v$) and area (A) of all simulated echotraces in the $\Delta\overline{S}_T \geq 2$ dB testing data set ($N = 8601$), (a–b) before and (c–d) after correction with the models of Table 3.

compensate for the range-dependent overestimation of school area (Figure 7b).

Discussion

The acoustic image observed on the echogram depends both on transducer and fish school characteristics, as well as on the processing threshold used to analyse the data. The acoustic beam is directive, thereby schools with a higher volume backscattering strength are sampled with an effectively wider beam angle. The same school can produce different echotraces when observed at different ranges due to beam spreading, and at any given range, the echotrace only represents an approximation of the true school dimensions, distorted to the discrete resolution of the echogram (Figure 2a and e). These issues are intrinsic to the acoustic measurement (Reid, 2000; Reid *et al.*, 2000; Diner, 2001) and must be accounted for in order to reliably infer the true shape, size, and density of schools from their observed echotraces; see, for example, Johannesson and Losse (1977), Kieser *et al.* (1993), Reid and Simmonds (1993), Reid *et al.* (2000), and Diner (2001, 2007) for related discussions or correction approaches with emphasis on vertical beaming.

Focusing on horizontal multi-beam observations, Misund (1990) proposed a formula for correcting the across-beam width of the school (Cw) based on the nominal beam width of the sonar. Vatnehol *et al.* (2017) used simulated multi-beam data and modified Misund's (1990) geometric model to also account for long-range distortions of Cw; a respective correction formula for school height was also produced by simulating the vertical insonification mode of the sonar. Applied to multi-beam horizontal area measurements (A_R) of the same school observed at different ranges (R), Misund *et al.* (1995) used the linear regression of $\sqrt{A_R}$ against R, and extrapolated it to the origin of the sonar beams to estimate the true value. This area correction approach makes no assumptions about the nominal beam width, but cannot handle a number of cases that often occur in horizontal multi-beam sampling. For example, the regression yields incorrect results if the proportion of the school that is being insonified changes with range, and is not applicable if the school area measured near the transducer is larger than the area measured at an outer position.

The simulation exercise investigated herein is an attempt to build sonar device-specific correction models that use the descriptors extracted from the observed echotrace as the only predictors of the true morphometric and energetic values of the insonified school. This implicitly assumes that, although the multi-beam sonar induces substantial intrinsic distortions to echotraces, the latter contain sufficient information to statistically infer the true properties of the school that is being sampled. The simulated scenarios included a broad range of school sizes and mean densities (1000 to 10000 m^2 and –42 to –33 dB, respectively) to increase variability in the source data, which, when combined with a tilted omnidirectional fan and constant school depth, ensured that partial (off-axis) insonification of schools was also included in the simulation.

Overall, the corrections significantly reduced the errors in the measured area and mean volume backscattering strength of echotraces, over the entire range of processing thresholds examined. The applicability limits of the method were empirically outlined via $\Delta\overline{S}_T$, which is also a quantity that can be computed from the observed echotrace, and is similar to the corresponding metric

Table 4. Mean absolute percentage errors $|\delta|$ (mean ± SD) of the corrected mean volume backscatter ($\bar{s}_{v,c}$) and area (A_c) of simulated echotraces in the $\Delta\overline{S}_T \geq 2$ dB testing data set, tabulated by true school area (A_0), true mean volume backscattering strength ($\overline{S}_{v,0}$), and processing threshold (T).

A_0 (m^2)		1000	5000	10 000	1000	5000	10 000
$\overline{S}_{v,0}$ (dB)	T (dB)	$\lvert\delta\bar{s}_{v,c}\rvert$ %			$\lvert\delta A_c\rvert$ %		
−42	**−53**	10.5 ± 4.0 (*3*)	6.3 ± 4.2 (*11*)	5.0 ± 7.5 (*17*)	7.0 ± 2.5	3.8 ± 1.9	2.4 ± 2.0
	−51	—	9.6 ± 3.8 (*9*)	6.5 ± 4.2 (*13*)	—	2.2 ± 1.6	4.2 ± 1.5
	−49	—	8.1 ± 3.3 (*6*)	8.7 ± 5.9 (*9*)	—	2.4 ± 1.4	4.5 ± 6.3
	−47	—	—	20.6 ± 1.5 (*3*)	—	—	8.0 ± 1.8
	All T[a]	13.4 ± 5.3 (*5*)	7.7 ± 4.1 (*44*)	7.9 ± 7.1 (*75*)	6.0 ± 2.3	3.0 ± 2.1	4.2 ± 4.2
−38	**−53**	8.7 ± 3.8 (*8*)	4.2 ± 4.2 (*17*)	3.9 ± 3.5 (*17*)	6.7 ± 4.7	4.7 ± 2.9	3.9 ± 3.0
	−51	6.9 ± 6.1 (*6*)	7.8 ± 8.0 (*16*)	4.3 ± 4.4 (*17*)	8.4 ± 5.0	4.2 ± 2.7	3.6 ± 2.5
	−49	9.1 ± 4.6 (*4*)	6.7 ± 6.7 (*12*)	8.1 ± 9.7 (*17*)	6.9 ± 2.5	4.6 ± 3.8	3.6 ± 2.6
	−47	—	7.1 ± 2.6 (*9*)	8.6 ± 5.7 (*14*)	—	3.9 ± 2.2	4.2 ± 3.1
	All T[a]	7.8 ± 4.6 (*31*)	6.2 ± 5.5 (*94*)	5.7 ± 6.1 (*114*)	7.5 ± 4.9	4.5 ± 2.9	3.6 ± 2.6
−33	**−53**	15.8 ± 8.5 (*17*)	4.6 ± 3.8 (*17*)	6.4 ± 4.6 (*17*)	31.4 ± 21.2	8.3 ± 4.8	15.0 ± 11.7
	−51	11.9 ± 9.4 (*13*)	3.3 ± 6.6 (*17*)	6.6 ± 6.6 (*17*)	13.4 ± 7.8	7.9 ± 2.9	9.4 ± 8.2
	−49	10.2 ± 7.1 (*9*)	4.2 ± 4.2 (*17*)	4.2 ± 4.3 (*17*)	4.7 ± 3.1	4.3 ± 2.7	3.2 ± 2.7
	−47	6.2 ± 5.1 (*8*)	6.3 ± 3.1 (*17*)	3.1 ± 2.5 (*17*)	3.3 ± 3.3	4.6 ± 2.6	1.8 ± 1.7
	All T[a]	12.2 ± 8.4 (*81*)	4.3 ± 4.0 (*119*)	5.0 ± 4.9 (*119*)	14.9 ± 15.1	6.1 ± 3.9	7.1 ± 8.2
All $\overline{S}_{v,0}$[b]		11.8 ± 8.0 (*396*)	5.1 ± 4.5 (*918*)	5.4 ± 5.4 (*1072*)	10.6 ± 9.5	4.9 ± 3.1	4.6 ± 4.8
Total[c]		6.4 ± 6.0 (*8601*)			5.2 ± 4.8		

All corrections derive from the models listed in Table 3; numbers in parentheses show the echotrace count (N) per category. Note that only selected thresholds T and $\overline{S}_{v,0}$ and A_0 classes are shown to reduce information density.

[a]Including the $T = [-52, -50, -48$ dB] levels not shown in this table.

[b]Including the $\overline{S}_{v,0} = [-41, -40, -39, -37, -36, -35, -34$ dB] classes not shown in this table.

[c]Including the $\overline{S}_{v,0}$ and $A_0 = [2000, 3000, 4000, 6000, 7000, 8000, 9000$ m^2] classes not shown in this table.

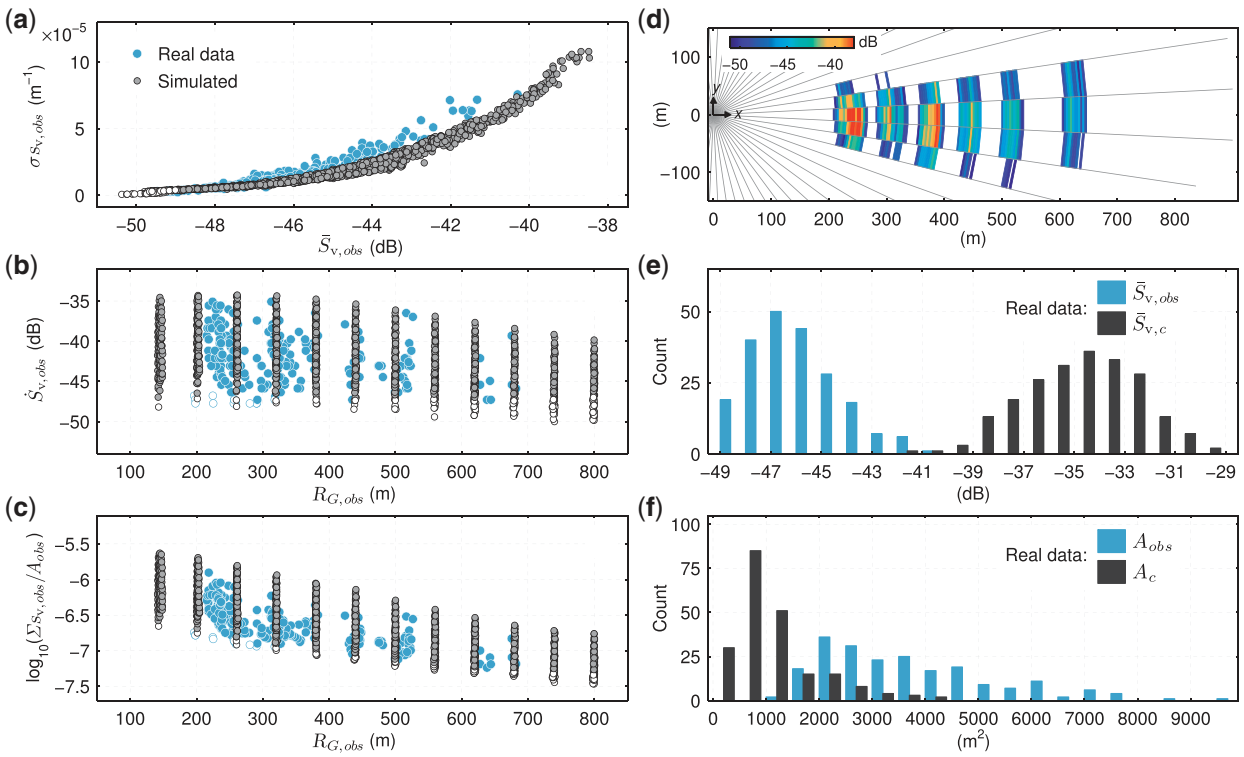

Figure 6. (a–c) Comparison of observed descriptors extracted from real and simulated echotraces; processing threshold T is −51 dB for both data categories. Open markers denote observations with $\Delta\overline{S}_T < 2$ dB. Simulated data include both training and testing observations and are only shown at selected distances from the transducer (140, 200, 260, . . ., 800 m) to reduce clutter. (d) Example real echotraces of the same school observed at different ranges ($T = -51$ dB). The echotraces are shown at their actual range, but for illustration purposes, their angular (across-beam) position has been rotated to align with the $+x$-axis. (e) Distribution of mean volume backscattering strength of real echotraces ($\Delta\overline{S}_T \geq 2$ dB, $N = 213$ detections), before ($\overline{S}_{v,obs}$) and after correction ($\overline{S}_{v,c}$); only real data plotted with closed markers in panels a–c were included in the corrections, using the models of Table 3. (f) As in panel e, but for echotrace area.

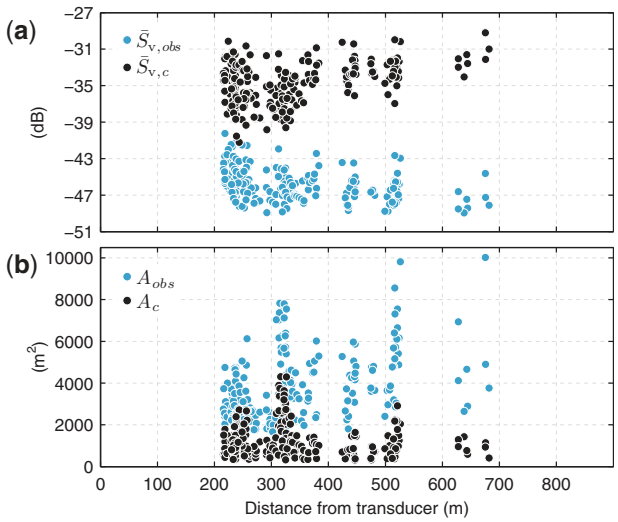

Figure 7. Scatter plots of observed and corrected (a) mean volume backscattering strength and (b) area of real echotraces with $\Delta\overline{S}_T \geq 2$ dB vs. their distance from the transducer (see also Supplementary Figure S2 for corresponding plots based on simulated data).

used in Diner's (2001) simulations. While the correction performance (see candidate models of Table 2) was superior when only echotraces with high signal-to-noise ratio were processed (meaning that their observed mean volume backscattering strength was at least 5–6 dB above the processing threshold), the analysis showed that a lower $\Delta\overline{S}_T$ criterion was sufficient for consistent results. Specifically, when echotraces with $\Delta\overline{S}_T < 2$ dB were filtered out, the corrections produced mean absolute percentage errors of 5.2% and 6.4% for A_c and $\bar{s}_{v,c}$, respectively. These area correction errors are very similar to those reported by Vatnehol *et al.* (2017) for the closely related (see Figure 2c and g) *Cw* descriptor measured with a Simrad SX90 sonar (Simrad, 2015a), although the two studies used different simulator and correction model designs to account for the systematic measurement errors.

Corrections could not be applied to echotraces representing fish schools that were located near the transducer, and were, as a result, severely under-sampled. Directing a tilted omnidirectional fan at fish schools that occupy a depth layer is a characteristic that underpins the sampling with horizontal sonar (Misund and Coetzee, 2000), but it inherently creates an asymmetrical sampling with range, unless a single school is selected and tracked by actively manipulating the tilt angle (Misund *et al.*, 1998). With respect to our simulations, this would correspond to a design that translated the schools away from the transducer while keeping them always on (or near) the acoustic axis. This sampling mode was partially represented in the more general simulation scenarios examined herein, where the centre of schools intersected the acoustic axis at a range of about 250–300 m from the transducer. While specific simulations are needed to conclude with confidence, the overall good performance of the corrections across a challenging mixture of on- and off-axis school insonifications suggests that the method investigated herein would also be applicable to sampling modes that actively modify the beam tilt angle to keep the tracked school on-axis.

In its current design, the simulator accounted for some of the systematic measurement errors involved in horizontal sonar sampling, i.e. those related to the beam pattern effect, the overlap of neighbouring beams, the polar geometry of the multi-beam echogram, and the spatial configuration of the tilted omnidirectional fan in relation to the location of fish schools. While the overall behaviour of the simulator was convincing and the systematic issues were reproduced well, the study did not consider environmental sources of variability or fish school behavioural aspects. For example, the simplified school model ignored fish polarization and its substantial effects on the recorded S_v (Boswell *et al.*, 2009; Holmin *et al.*, 2012), while the allocation of voxel backscatter had no spatial correlation within the school, thus dense regions or vacuoles that emerge in schooling fish (Fréon *et al.*, 1992; Gerlotto *et al.*, 2006; Guillard *et al.*, 2011) were not represented in the simulations. Furthermore, this internal structure remained static across all insonification positions, and the general shape of the school was fixed to an idealized oblate spheroid. Fish schools are in fact dynamic structures (Misund, 1993) that can present substantial temporal fluctuations in their cross-sectional area (Trygonis *et al.*, 2016), while their vertical or horizontal dynamics introduce additional uncertainties due to the variable position of the schools' gravity centre relative to the acoustic axis (Brehmer *et al.*, 2006). In addition, the actual *in situ* sampling schemes used to collect the sonar data may also impact the observed fish school descriptors. For example, Brehmer *et al.* (2002, 2006) proposed that school area can be approximated through the along-beam width (*Lw*) of the school, by assuming a spherical school shape that has a diameter equal to *Lw*. Yet, a different variant of *Lw* was appropriate (i.e. the mean or maximum *Lw*) depending on whether data were recorded from a free-drifting vessel or from one that moved along a transect line or adapted its course to actively follow a school.

Given the enormous complexity of modelling all dynamic and behavioural aspects in a single simulation, several simplifications were made to both transducer and school model properties. The systematic sources of bias, however, that were integrated into the analysis were not trivial, and by themselves, contributed to mean absolute percentage errors in the order of 100% and 80% in the observed area and mean volume backscatter, respectively, as per the simulated $\Delta\overline{S}_T \geq 2$ dB testing data set. Of course, simplifications increase discrepancies between the simulated and real system, and indeed, Figure 6a shows that, for the same observed mean volume backscattering strength, the echotraces currently generated by the simulator have smaller variance than the real ones. However, overall, the side-by-side comparison of simulated vs. real echotrace descriptors revealed no anomalous behaviour in the former, increasing confidence in the validity of the simulation engine. The experimental application of corrections to real SP90 data also yielded a pattern in the corrected descriptors that was concordant to the one expected by the simulations, but there was no means to ground truth the true properties of real fish schools. Therefore, it is not possible to assess the errors in the corrected real data.

Using a calibrated sonar (Foote *et al.*, 2005; Demer *et al.*, 2015; Macaulay *et al.*, 2016) for the comparisons and implementing its actual directivity in the simulator is necessary to obtain more precise results. Moreover, incorporating dynamic aspects in the internal structure and motion of schools, and expanding the simulation scenarios to cover multiple sonar settings and school sizes will increase the fidelity of the simulated system and the applicability of generated correction models to a broader range of real data. This is of particular importance, given that the

correction models established herein are based on observed descriptors, which in turn depend on the properties of the simulated schools and transducer. In addition, the models significantly reduce the observed errors through a linear combination of the distorted echotrace descriptors, but provide no insight on the relative importance of the sources of bias that actually caused that distortion. Therefore, and as in all simulation attempts, the resulting correction models are applicable only to data from a similar sonar and fish school size/density properties as those used in the simulations that produced them.

New fishery sonars like the Simrad SX90 or SU90 (Simrad, 2015b) have identical frequency range and similar spatial configuration of beams with the SP90 (i.e. cylindrical transducer and 64 beams arranged in an omnidirectional fan), but narrower beam widths. The methodological framework of the correction models suggests that a similar approach can be applied to these sonars, and future work should expand the simulations on these devices. Notwithstanding complexities pertaining to the target strength of schooling fish in the lateral aspect (Cutter and Demer, 2007; Tang *et al.*, 2009), this will help establish more general solutions to the multi-parametric problem of debiasing fish school descriptors, in order to convert the corrected mean volume backscattering strength of schools to absolute fish density estimates.

Supplementary data

Supplementary material is available at the *ICESJMS* online version of the article.

Acknowledgements

We thank Stratis Georgakarakos for his advice during development of the simulator. Two anonymous reviewers and Patrice Brehmer provided very helpful comments on this manuscript.

References

Aglen, A. 1983. Echo integrator threshold and fish density distribution. FAO Fisheries Reports, 300: 35–44.

Bahri, T., and Fréon, P. 2000. Spatial structure of coastal pelagic schools descriptors in the Mediterranean Sea. Fisheries Research, 48: 157–166.

Boswell, K. M., Roth, B. M., and Cowan, J. H. Jr 2009. Simulating the effects of side-aspect fish orientation on acoustic biomass estimates. ICES Journal of Marine Science, 66: 1398–1403.

Brehmer, P., Georgakarakos, S., Josse, E., Trygonis, V., and Dalen, J. 2007. Adaptation of fisheries sonar for monitoring schools of large pelagic fish: dependence of schooling behaviour on fish finding efficiency. Aquatic Living Resources, 20: 377–384.

Brehmer, P., Gerlotto, F., and Rouault, A. 2002. Inter-standardisation of acoustic devices: an integrated fish school database for behavioural studies. Acta Acoustica, 88: 730–734.

Brehmer, P., Josse, E., and Nøttestad, L. 2012. Evidence that whales (*Balaenoptera borealis*) visit drifting fish aggregating devices: do their presence affect the processes underlying fish aggregation? Marine Ecology, 33: 176–182.

Brehmer, P., Lafont, T., Georgakarakos, S., Josse, E., Gerlotto, F., and Collet, C. 2006. Omnidirectional multibeam sonar monitoring: applications in fisheries science. Fish and Fisheries, 7: 165–179.

Castillo, J., and Robotham, H. 2004. Spatial structure and geometry of schools of sardine (*Sardinops sagax*) in relation to abundance, fishing effort, and catch in northern Chile. ICES Journal of Marine Science, 61: 1113–1119.

Coetzee, J. 2000. Use of a shoal analysis and patch estimation system (SHAPES) to characterise sardine schools. Aquatic Living Resources, 13: 1–10.

Cutter, G. R., and Demer, D. A. 2007. Accounting for scattering directivity and fish behaviour in multibeam-echosounder surveys. ICES Journal of Marine Science, 64: 1664–1674.

Demer, D. A., Berger, L., Bernasconi, M., Bethke, E., Boswell, K., Chu, D., Domokos, R., *et al.* 2015. Calibration of acoustic instruments. ICES Cooperative Research, Report No. 326. 133 pp.

Diner, N. 2001. Correction on school geometry and density: approach based on acoustic image simulation. Aquatic Living Resources, 14: 211–222.

Diner, N. 2007. Evaluating uncertainty in measurements of fish shoal aggregate backscattering cross-section caused by small shoal size relative to beam width. Aquatic Living Resources, 20: 117–121.

Fernandes, P. G. 2009. Classification trees for species identification of fish-school echotraces. ICES Journal of Marine Science, 66: 1073–1080.

Foote, K. G., Chu, D., Hammar, T. R., Baldwin, K. C., Mayer, L. A., Hufnagle, L. C., Jr, and Jech, J. M. 2005. Protocols for calibrating multibeam sonar. Journal of the Acoustical Society of America, 117: 2013–2027.

Fréon, P., Gerlotto, F., and Soria, M. 1992. Changes in school structure according to external stimuli: description and influence on acoustic assessment. Fisheries Research, 15: 45–66.

Fréon, P., Gerlotto, F., and Soria, M. 1996. Diel variability of school structure with special reference to transition periods. ICES Journal of Marine Science, 53: 459–464.

Fritsch, F. N., and Carlson, R. E. 1980. Monotone piecewise cubic interpolation. SIAM Journal on Numerical Analysis, 17: 238–246.

Gerlotto, F., Bertrand, S., Bez, N., and Gutierrez, M. 2006. Waves of agitation inside anchovy schools observed with multibeam sonar: a way to transmit information in response to predation. ICES Journal of Marine Science, 63: 1405–1417.

Gerlotto, F., and Paramo, J. 2003. The three-dimensional morphology and internal structure of clupeid schools as observed using vertical scanning multibeam sonar. Aquatic Living Resources, 16: 113–122.

Guillard, J., Fernandes, P., Laloë, T., and Brehmer, P. 2011. Three-dimensional internal spatial structure of young-of-the-year pelagic freshwater fish provides evidence for the identification of fish school species. Limnology and Oceanography: Methods, 9: 322–328.

Hafsteinsson, M. T., and Misund, O. A. 1995. Recording the migration behaviour of fish schools by multi-beam sonar during conventional acoustic surveys. ICES Journal of Marine Science, 52: 915–924.

Haralabous, J., and Georgakarakos, S. 1996. Artificial neural networks as a tool for species identification of fish schools. ICES Journal of Marine Science, 53: 173–180.

Holmin, A. J., Handegard, N. O., Korneliussen, R. J., and Tjøstheim, D. 2012. Simulations of multi-beam sonar echos from schooling individual fish in a quiet environment. Journal of the Acoustical Society of America, 132: 3720–3734.

Johannesson, K. A., and Losse, G. F. 1977. Methodology of acoustic estimations of fish abundance in some UNDP/FAO resource survey projects. Rapports Et Procès-Verbaux Des Réunions Du Conseil International Pour L'Exploration De La Mer, 170: 296–318.

Kieser, R., Mulligan, T. J., Richards, L. J., and Leaman, B. M. 1993. Bias correction of rockfish school cross section widths from digitized echo sounder data. Canadian Journal of Fisheries and Aquatic Sciences, 50: 1801–1811.

Kvamme, C., Nøttestad, L., Fernö, A., Misund, O. A., Dommasnes, A., Axelsen, B. E., Dalpadado, P., *et al.* 2003. Migration patterns in Norwegian spring-spawning herring: why young fish swim away from the wintering area in late summer. Marine Ecology Progress Series, 247: 197–210.

Lawson, G. L., Barange, M., and Fréon, P. 2001. Species identification of pelagic fish schools on the South African continental shelf

using acoustic descriptors and ancillary information. ICES Journal of Marine Science, 58: 275–287.

Macaulay, G. J., Vatnehol, S., Gammelsæter, O. B., Peña, H., and Ona, E. 2016. Practical calibration of ship-mounted omni-directional fisheries sonars. Methods in Oceanography, 17: 206–220.

MacLennan, D. N., Fernandes, P. G., and Dalen, J. 2002. A consistent approach to definitions and symbols in fisheries acoustics. ICES Journal of Marine Science, 59: 365–369.

McClatchie, S., Thorne, R. E., Grimes, P., and Hanchet, S. 2000. Ground truth and target identification for fisheries acoustics. Fisheries Research, 47: 173–191.

Misund, O. A. 1990. Sonar observations of schooling herring: school dimensions, swimming behaviour, and avoidance of vessel and purse seine. Rapports Et Procès-Verbaux Des Réunions Du Conseil International Pour L'Exploration De La Mer, 189: 135–146.

Misund, O. A. 1993. Dynamics of moving masses: variability in packing density, shape, and size among herring, sprat, and saithe schools. ICES Journal of Marine Science, 50: 145–160.

Misund, O. A. 1997. Underwater acoustics in marine fisheries and fisheries research. Reviews in Fish Biology and Fisheries, 7: 1–34.

Misund, O. A., Aglen, A., and Frønæs, E. 1995. Mapping the shape, size, and density of fish schools by echo integration and a high-resolution sonar. ICES Journal of Marine Science, 52: 11–20.

Misund, O. A., Aglen, A., Hamre, J., Ona, E., Røttingen, I., Skagen, D., and Valdemarsen, J. W. 1996. Improved mapping of schooling fish near the surface: comparison of abundance estimates obtained by sonar and echo integration. ICES Journal of Marine Science, 53: 383–388.

Misund, O. A., and Coetzee, J. 2000. Recording fish schools by multi-beam sonar: potential for validating and supplementing echo integration recordings of schooling fish. Fisheries Research, 47: 149–159.

Misund, O. A., Fernö, A., Pitcher, T., and Totland, B. 1998. Tracking herring schools with a high resolution sonar. Variations in horizontal area and relative echo intensity. ICES Journal of Marine Science, 55: 58–66.

Olsen, S. 1969. A note on estimating school size from echo-traces. FAO Fisheries Reports, 78: 37–48.

Peña, H., Handegard, N. O., and Ona, E. 2013. Feeding herring schools do not react to seismic airgun surveys. ICES Journal of Marine Science, 70: 1174–1180.

Peraltilla, S., and Bertrand, S. 2014. *In situ* measurements of the speed of Peruvian anchovy schools. Fisheries Research, 149: 92–94.

Petitgas, P. 2003. A method for the identification and characterization of clusters of schools along the transect lines of fisheries-acoustic surveys. ICES Journal of Marine Science, 60: 872–884.

Petitgas, P., Massé, J., Beillois, P., Lebarbier, E., and Le Cann, A. 2003. Sampling variance of species identification in fisheries-acoustic surveys based on automated procedures associating acoustic images and trawl hauls. ICES Journal of Marine Science, 60: 437–445.

Petitgas, P., Reid, D. G., Carrera, P., Iglesias, M., Georgakarakos, S., Liorzou, B., and Massé, J. 2001. On the relation between schools, clusters of schools, and abundance in pelagic fish stocks. ICES Journal of Marine Science, 58: 1150–1160.

Reid, D. G. 2000. Report on echo trace classification. ICES Cooperative Research, Report No. 238. 107 pp.

Reid, D. G., Scalabrin, C., Petitgas, P., Massé, J., Aukland, R., Carrera, P., and Georgakarakos, S. 2000. Standard protocols for the analysis of school based data from echo sounder surveys. Fisheries Research, 47: 125–136.

Reid, D. G., and Simmonds, E. J. 1993. Image analysis techniques for the study of fish school structure from acoustic survey data. Canadian Journal of Fisheries and Aquatic Sciences, 50: 886–893.

Scalabrin, C., and Massé, J. 1993. Acoustical detection of the spatial and temporal distribution of fish shoals in the Bay of Biscay. Aquatic Living Resources, 6: 269–283.

Simmonds, J., and MacLennan, D. 2005. Fisheries Acoustics, 2nd edn. Chapman & Hall, London.

Simrad. 2007. Simrad SP90 low frequency long range fishery sonar; Operator manual. 850-164511/Rev.F, Horten, Norway.

Simrad. 2015a. Simrad SX90; Operator manual. 307672/Rev.G, Horten, Norway.

Simrad. 2015b. Simrad SU90; Operator manual. 381291/Rev.B, Horten, Norway.

Soria, M., Bahri, T., and Gerlotto, F. 2003. Effect of external factors (environment and survey vessel) on fish school characteristics observed by echosounder and multibeam sonar in the Mediterranean Sea. Aquatic Living Resources, 16: 145–157.

Stockwell, J. D., Weber, T. C., Baukus, A. J., and Jech, J. M. 2013. On the use of omnidirectional sonars and downwards-looking echosounders to assess pelagic fish distributions during and after midwater trawling. ICES Journal of Marine Science, 70: 196–203.

Tang, Y., Nishimori, Y., and Furusawa, M. 2009. The average three-dimensional target strength of fish by spheroid model for sonar surveys. ICES Journal of Marine Science, 66: 1176–1183.

Trenkel, V. M., Berger, L., Bourguignon, S., Doray, M., Fablet, R., Massé, J., Mazauric, V., *et al.* 2009. Overview of recent progress in fisheries acoustics made by Ifremer with examples from the Bay of Biscay. Aquatic Living Resources, 22: 433–445.

Trygonis, V., Georgakarakos, S., Dagorn, L., and Brehmer, P. 2016. Spatiotemporal distribution of fish schools around drifting fish aggregating devices. Fisheries Research, 177: 39–49.

Trygonis, V., Georgakarakos, S., and Simmonds, E. J. 2009. An operational system for automatic school identification on multibeam sonar echoes. ICES Journal of Marine Science, 66: 935–949.

Tsagarakis, K., Giannoulaki, M., Somarakis, S., and Machias, A. 2012. Variability in positional, energetic and morphometric descriptors of European anchovy *Engraulis encrasicolus* schools related to patterns of diurnal vertical migration. Marine Ecology Progress Series, 446: 243–258.

Uranga, J., Arrizabalaga, H., Boyra, G., Hernandez, M. C., Goñi, N., Arregui, I., Fernandes, J. A., *et al.* 2017. Detecting the presence-absence of blue fin tuna by automated analysis of medium-range sonars on fishing vessels. PLoS One, 12: e0171382.

Vatnehol, S., Peña, H., and Ona, E. 2017. Estimating the volumes of fish schools from observations with multi-beam sonars. ICES Journal of Marine Science, 74: 813–821.

Weill, A., Scalabrin, C., and Diner, N. 1993. MOVIES-B: an acoustic detection description software. Application to shoal species' classification. Aquatic Living Resources, 6: 255–267.

Zwolinski, J., Morais, A., Marques, V., Stratoudakis, Y., and Fernandes, P. G. 2007. Diel variation in the vertical distribution and schooling behaviour of sardine (*Sardina pilchardus*) off Portugal. ICES Journal of Marine Science, 64: 963–972.

Handling editor: David Demer